Electron density of $CaNi_2Si_2$ studied using synchrotron x-ray diffraction and first-principles calculations

2000 J. Phys.: Condens. Matter 12 2667

(http://iopscience.iop.org/0953-8984/12/12/308)

J. Phys.: Condens. Matter **12** (2000) 2667–2679. Printed in the UK PII: S0953-8984(00)06419-5

Electron density of $CaNi_2Si_2$ studied using synchrotron x-ray diffraction and first-principles calculations

G Gavoille†¶, N K Hansen†, R Welter‡, B Malaman‡, P Herzig§ and H-G Krane‖

† Laboratoire de Cristallographie et Modélisation des Matériaux Minéraux et Biologiques, UPRESA-CNRS-7036, Université Henri Poincaré, BP 239, F-54506 Vandoeuvre-lès-Nancy Cédex, France

‡ Laboratoire de Chimie du Solide Minéral, UMR-CNRS-7555, Université Henri Poincaré, BP 239, F-54506 Vandoeuvre-lès-Nancy Cédex, France

§ Institut für Physikalische Chemie, Universität Wien, Währingerstraße 42, A-1090 Vienna, Austria

‖ Mineralogisch-Petrologisches Institut, Universität Bonn, Poppelsdorfer Schloß, D-53115 Bonn, Germany

Received 29 July 1999, in final form 10 January 2000

Abstract. The electron-density distribution in $CaNi_2Si_2$ has been analysed by means of x-ray diffraction measurements and a full-potential augmented-plane-wave band-structure calculation. The agreement between experiment and theory is good, considering the difficulty of the experiment. A Si–Si bonding interaction is clearly observed in the valence electron distribution as well as a preferred occupation of the Ni 3d orbitals.

1. Introduction

The $ThCr_2Si_2$-type structure ($I4/mmm$, space group No 139) [1] is one of the most frequently observed structures in ternary compounds with the formula RT_2X_2 (R: alkaline earth or lanthanide element; T: transition metal; X: element from group 13 to 16). During the past few decades, quite a number of physical observations and studies have been devoted to these compounds [2], investigating features such as superconductivity, valence fluctuation, mixed valency [3] and heavy-fermion behaviour [4], as well as a wide range of magnetic properties [5–8]. If the magnetism of the silicides is considered, among the transition metals only Mn carries a magnetic moment, but strong transferred hyperfine fields have been observed in Fe when R is a lanthanide element, showing that iron is nearly magnetic in these compounds. This emphasizes the importance of the filling of the 3d band for the magnetic properties. As regards the Mn-based compounds, a great variety in the magnetic behaviour has been observed, ranging from ferromagnetism to antiferromagnetism and canted magnetic structures, some of which exhibit a transition from ferromagnetism to antiferromagnetism when the temperature increases. This may result from a complex Fermi surface which may be very sensitive to the interatomic distances, as proved by the recent magnetic study of the $La_{1-x}Y_xMn_2Ge_2$ solid solution [9], where the magnetic ground state evolves from ferromagnetism to antiferromagnetism when x increases. Hence, seven different Mn-sublattice magnetic arrangements have been encountered in the x–T diagram [9].

¶ Deceased January 1999.

0953-8984/00/122667+13$30.00

The RT_2X_2 structure is layered, with R–X–T_2–X–R–X–T_2–X–R planes stacked along the c-axis. All of the atoms are located at special positions, R at 2a (0, 0, 0), T at 4d ($\frac{1}{2}$, 0, $\frac{1}{4}$) and X at 4e (0, 0, z) with z always close to 0.37, and consequently the distances mainly depend on the a- and c-parameters. The understanding of the magnetic properties now requires complete knowledge of the band structure. Some band-structure calculations were based on an extended Hückel method [10], but a self-consistent calculation using the KKR method with an exchange–correlation potential using the local spin-density approximation was carried out on YMn_2Ge_2, $LaMn_2Ge_2$ and $LaCo_2Ge_2$ [11]. The calculated magnetic moment of Mn in $LaMn_2Ge_2$ significantly differs from the experimental value. Recently, calculations concerning $CaFe_2P_2$, $CaNi_2P_2$, $SrFe_2P_2$ and $BaFe_2P_2$ [12, 13] used the full-potential augmented-plane-wave (FLAPW) method [14] with a Hedin–Lundqvist exchange–correlation potential [15]. The band structures of these latter compounds are qualitatively similar for the transition metal 3d bands.

Our aim is an experimental determination of the electron density of the RT_2X_2 compounds for different fillings of the 3d band using x-ray diffraction experiments. These results are compared with theoretical studies, and they may provide the distribution of the 3d electrons over the different orbitals and then the anisotropy of the electron density. In the present paper, we report on the first experiment performed on the paramagnetic compound $CaNi_2Si_2$. The reliability of the results is considered and, especially, the consequence of the lack of sensitivity of the diffraction experiment to diffuse electron-density distributions is discussed. The experimental results are also compared with results from a FLAPW calculation.

2. Experimental procedure

The sample was prepared from commercially available high-purity elements: Ca (pieces, 99.9%), Ni (powder, 99.99%) and Si (pieces, 99.99%). A pellet of stoichiometric mixture was melted in an induction furnace and annealed for ten days at 1273 K.

A single crystal was extracted from the resulting ingots and studied first on a Weissenberg camera (Cu Kα). It had an irregular shape with a maximum dimension of about 0.03 mm.

The intensity data were collected at HASYLAB on the four-circle diffractometer D3 at room temperature.

Because of the very small size of the sample, reflected intensities were very weak, no primary beam attenuation was needed and the counter dead-time corrections were negligibly small. The incident beam intensity was monitored by two detectors (count rates: C_h and C_v) which allows a correction for its total intensity fluctuations and for fluctuations of its polarization ratio. These corrections were applied to each individual profile according to

$$I_{corr} = I_{integr} S/\mathrm{LP}$$

with

$$\mathrm{LP} = \frac{(1+Q) + (1-Q)\cos^2 2\theta}{2\sin 2\theta}$$

$$S = \frac{1}{\langle C_h \rangle + \langle C_v \rangle}$$

$$Q = \frac{\langle C_h \rangle - \langle C_v \rangle}{\langle C_h \rangle + \langle C_v \rangle}.$$

S scales the intensities according to the total monitor counts, LP is the Lorentz and polarization correction.

In addition to the direct monitoring of the incident x-ray beam, the intensities of two standard reflections were measured every 40 minutes. Their variations were described by a cubic spline function allowing an average deviation of 1.67 standard deviations from the fit, and the data corrected in consequence thereof.

The experimental conditions are summarized in table 1.

Table 1. Experimental conditions.

Wavelength (Å)	0.399
Unit-cell parameters (Å):	
a	3.987(1)
c	9.672(2)
Scan mode	ω-step scan
Steps per scan	81
Step width	0.012°
Counting	1 s/step
Standard reflections	040 and 228
Maximum 2ϑ	60°
$((\sin\vartheta)/\lambda)_{max}$	1.09 Å^{-1}
Total number of reflections	3103
Number of unique reflections	283
Internal agreement indices[a]:	
R_w	4.0%
Z	0.85

[a] R_w is an R-factor and Z a normalized χ^2-estimator [16].

Collecting a full sphere of data means that between 8 and 16 equivalents or duplicates were measured for most of the unique reflections, and each one at very different times during the experiment. The computer program SORTAV [16] was used for the merging of the equivalent reflections. The agreement between the estimated standard errors of the individual reflection intensities and the dispersion among equivalent reflections was good, as indicated by the χ^2-estimator.

3. Crystal structure and electron-density modelling

In $CaNi_2Si_2$, all the atoms occupy special positions, which has the consequence that the structure factor expression may be simplified for different groups of reflections, and, as we shall see, results in there being certain limitations on what information can be reliably extracted from the x-ray diffraction intensities.

In figure 1 one unit cell is shown. The following structural characteristics should be stressed:

- The shortest Ni–Ni distance is 2.819 Å.
- The nickel atoms are tetrahedrally coordinated by silicon at a distance of 2.312 Å.
- The silicon atoms can be considered to have a square-planar pyramidal coordination (four Si in the base and another Si at the top); the shortest Si–Si distance (2.49 Å) is almost as short as in pure silicon single crystals (2.35 Å).
- The Ca coordination may be considered tenfold with respect to the Si atoms (this is only of marginal interest for our discussion).

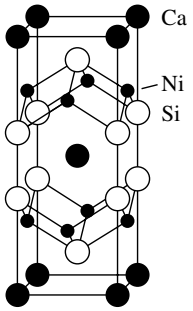

Figure 1. The unit cell of $CaNi_2Si_2$.

The positions of the atoms in the cell are

Ca:	$0, 0, 0$	
Ni:	$\frac{1}{2}, 0, \frac{1}{4}$	
Si:	$0, 0, z$	with $z \approx \frac{3}{8}$.

In our study we find $z = 0.3711(1)$.

For the analysis of the x-ray data we use a so-called multipole model [17]; the total electron density is written as the sum of atomic-like densities, ρ_k, each given by a limited expansion in spherical harmonic functions in real form† which, when multiplied by a radial function R_{kl}, form a 'multipole'.

For Ni,

$$\rho_{\mathrm{Ni}}(\boldsymbol{r}) = \rho_{\mathrm{Ni,core}}(r) + P_{\mathrm{Ni}\,4s}\,\rho_{\mathrm{Ni}\,4s}(r) + \sum_{l=0}^{4,\,l\ \mathrm{even}} \kappa'^{3}\rho_{\mathrm{Ni}\,3d}(\kappa' r) \sum_{m=-l}^{l} P_{\mathrm{Ni}\,lm}\, y_{lm}(\boldsymbol{r}/r).$$

The only terms contributing to the density because of the site symmetry ($\bar{4}m2$) are $(l, m) =$ (0, 0), (2, 0), (3, 2+), (4, 0) and (4, 4+). We neglect the possible contribution from (3, 2+) (see below).

For Si,

$$\rho_{\mathrm{Si}}(\boldsymbol{r}) = \rho_{\mathrm{Si,core}}(r) + P_{\mathrm{Si}\,V}\kappa^{3}\rho_{\mathrm{Si,valence}}(\kappa r) + \sum_{l=1}^{4} \kappa'^{3} R_{\mathrm{Si}\,l}(\kappa' r) \sum_{m=-l}^{l} P_{\mathrm{Si}\,lm}\, y_{lm}(\boldsymbol{r}/r)$$

which has a site symmetry $4mm$, the contributing multipoles are $(l, m) = (0, 0)$, (1, 0), (2, 0), (3, 0), (4, 0) and (4, 4+). $\rho_{\mathrm{Ni,core}}$, $\rho_{\mathrm{Si,core}}$, $\rho_{\mathrm{Ni}\,4s}$, $\rho_{\mathrm{Ni}\,3d}$ and $\rho_{\mathrm{Si,valence}}$ are spherically averaged Hartree–Fock core and valence electron densities of the appropriate atom orbitals; $\rho_{\mathrm{Si,valence}}$ is the average of the 3s and 3p orbitals of the ground state of the isolated atom.

For silicon we adopt functions of the form $R_{\mathrm{Si}\,l}(r) \sim r^{n_l}\exp(-\zeta r)$, whereas for Ni we use the square of the radial part of the 3d Hartree–Fock orbitals [18] for l even. κ and κ' control a possible expansion/contraction of the radial functions. $P_{k\,V}$ and $P_{k\,lm}$ are expansion coefficients (population parameters). The spherical harmonic functions are expressed relative to orthonormal coordinate systems which, for all of the atoms, have been chosen with their axes parallel to the unit-cell axes.

The thermal motions of the atoms are treated within the convolution approximation, and supposed to be harmonic.

† y_{lm} is a product of an associated Legendre polynomial multiplied by a cosine or sine function when m is positive or negative, respectively.

The form factors corresponding to the above atomic electron-density expressions take much the same form [17]. In the multipole expansion we may distinguish two types of term depending on the parity under inversion, and denote the corresponding contributions to the form factor as f^c and f^{ac}, such that the form factor takes the form: $f = f^c + \mathrm{i}f^{ac}$ [19]. This division also corresponds to the parity of the order l of the multipoles.

According to the value of the reflection index l, the structure factor may be expressed as follows:

(i) $h + k$ odd and $l = 8n \pm 1$ (intensity very weak):

$$F(\boldsymbol{H}) = 2f_{\mathrm{Ca}} - 4f^{ac}_{\mathrm{Ni}} - 2\sqrt{2}f^{c}_{\mathrm{Si}} \pm 2\sqrt{2}f^{ac}_{\mathrm{Si}}.$$

(ii) $h + k$ odd and $l = 8n \pm 3$ (medium intensity):

$$F(\boldsymbol{H}) = 2f_{\mathrm{Ca}} + 4f^{ac}_{\mathrm{Ni}} + 2\sqrt{2}f^{c}_{\mathrm{Si}} \pm 2\sqrt{2}f^{ac}_{\mathrm{Si}}.$$

(iii) $h + k$ even and $l = 4n$ (intensity strong):

$$F(\boldsymbol{H}) = 2f_{\mathrm{Ca}} + (-1)^h 4f^{c}_{\mathrm{Ni}} + (-1)^n 4f^{c}_{\mathrm{Si}}.$$

(iv) $h + k$ even and $l = 4n + 2$ (intensity strong):

$$F(\boldsymbol{H}) = 2f_{\mathrm{Ca}} - (-1)^h 4f^{c}_{\mathrm{Ni}} - (-1)^n 4f^{c}_{\mathrm{Si}}.$$

Looking at the actual data, the measured intensities of the first group of reflections are hardly ever found to be significantly different from zero and, compared to the structure factors calculated from the refined models, they are often too strong (we will return to this point).

In the final model we assumed the calcium contribution to be that of the free divalent ion. No other scheme significantly improved the fit to the data.

For Ni we consider that the centrosymmetric component of the valence density can be decomposed into a contribution from atomic-like 3d–3d orbital products, a diffuse valence contribution arising from 4s- and 4p-like states and, finally, 4s–3d orbital products due to hybridization. Except for the first term, these will affect the diffraction very faintly, and we do not take them into account. f^{ac}_{Ni} will arise from 3d–4p-like orbital products which are also expected to be diffuse and thus not contribute much to the diffraction. It is to be stressed that f^{c}_{Ni} and f^{ac}_{Ni} contribute to different reflections, thus making a separation of the effects safer.

The valence shell electron density of silicon is rather diffuse and contributes little to the scattering of the x-rays. Having no precise idea of the actual oxidation state of these atoms, it is difficult to make an *a priori* guess about reasonable radial functions in the multipole model, and the refinements lead to parameters with quite large standard deviations. We therefore used two criteria for establishing a multipole model density: refinements were carried through to convergence for different radial functions R_l; and *a posteriori* we tested whether the valence density was positive. An optimum result was obtained for:

$$n_l = 4, 4, 6, 8 \qquad \text{for } l = 1, 2, 3, 4 \qquad \text{and } \zeta = 2.0 \text{ Bohr}^{-1}.$$

One of the basic problems with this structure is that the calcium ions contribute with full weight to all reflections, and to a vast extent overshadow finer details in the electron-density distribution of the other atoms.

In the final refinements, the following parameters were optimized: anisotropic thermal displacement parameters (two per atom because of the site symmetries); the z-coordinate of Si; the multipole populations corresponding to the Ni 3d orbital products (four parameters); and the radial contraction parameter κ'. Furthermore, so were all site-symmetry-allowed multipole populations of Si (4*mm* symmetry), i.e. five parameters in addition to a κ.

In table 2 we give the agreement indices of the final multipole model. A comparison with a standard 'independent-atom model' shows that the data do contain information going beyond this rather primitive description of the electron density in the crystal.

For the multipole refinement we have given the results (i) when only refining the reflections having an intensity which is significantly above zero ($I > 3\sigma(I)$) and (ii) when refining all measured reflections. We note that the parameters resulting from these two refinements agree within their random errors.

Table 2. Agreement indices. (Notes: IAM: results for *independent-atom* form factors. Standard agreement factors as calculated with the structure factor moduli $R(F)$, with their squares $R(F^2)$ or using the weighting scheme $R_w(F^2)$ in the refinement. 'G.o.F.' is the root of the normalized χ^2-deviation between observed and calculated squares of the structure factors (F^2).)

		Multipole model	
	IAM	$I > 3\sigma(I)$	All data
$R(F)$ (%)	1.7	1.4	5.2
$R(F^2)$ (%)	2.2	1.5	1.9
$R_w(F^2)$ (%)	2.4	1.7	1.8
G.o.F.	1.79	1.31	1.14

The total valence density may be calculated directly from the model described earlier. Very often bonding is illustrated by deformation-density mapping; the 'deformation density' is defined as the difference between the total electron density in the crystal and the superposition of independent, spherically averaged atom densities (figure 2). This function may either be

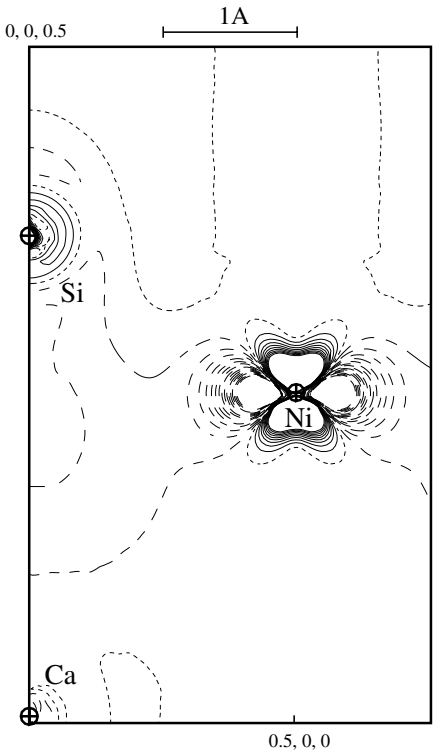

Figure 2. The experimental deformation density for $CaNi_2Si_2$ in the (100) plane. A linear mesh of contour lines (distance: 0.1 electrons Å^{-3}) is used.

calculated by a Fourier synthesis, using observed or model structure factors, or from the multipole model density expression. In the latter case the effect of atomic thermal vibrations is deconvoluted within a rigid pseudo-atom approximation.

4. Band-structure calculation

The experimental results are compared with a calculation of the electronic band structure using a FLAPW method [14] with a Hedin–Lundqvist exchange–correlation potential [15]. For the l-expansion of the potential and the electron density, within the muffin-tin spheres, terms up to $l = 8$ were taken into account. For the wavefunctions, plane waves in the interstitial region were included up to a length of $42\pi/a$. The chosen plane-wave basis corresponds to approximately 560 basis functions. The self-consistency procedure has been performed with 330 $\boldsymbol{k}$-points in the irreducible part of the Brillouin zone (BZ). The same mesh of $\boldsymbol{k}$-points has also been used for the calculation of the electron densities. The BZ integration was performed by means of the linearized tetrahedron method [21]. The muffin-tin radii were chosen as 3 au for Ca and 2 au for both Ni and Si.

Figure 3 shows the total density of states (DOS) and the most important local l-like components, i.e. Si s and p, Ni d as well as the Ca s, p and d components. Starting at the low-energy side, the first double peak has mainly Si s character and corresponds to bonding and antibonding Si–Si s–s σ-bonds. The peak complex that follows after a gap of $\approx$0.1 Ryd is due to overlapping Si p and Ni d states. The Ni d states near the Fermi level, which are occupied to a large extent, can be shown to have mainly antibonding character since the bonds between neighbouring Ni atoms are involved. The DOS reflects the essential bonding properties of this compound, namely strong covalent bonds between the Si atoms at a distance of 2.49 Å and also between the Si atoms and the Ni atoms, while for all Ni compounds with $ThCr_2Si_2$ structure the strength of the bonds between neighbouring transition metals is reduced compared to that for the corresponding Fe and Co compounds because of the occupation of antibonding d states. The local partial DOS components in the Ca sphere show small but important contributions to the total DOS of this compound over the whole energy range. The corresponding occupied states are involved in covalent Ca–Ni, Ca–Ca and Ca–P bonds. A more detailed discussion of the influence of Ca d (s, p) states on the analogous compound $CaNi_2P_2$, for which the bonding situation is rather similar, can be found in reference [12].

5. Results and discussion

We will discuss the results in two ways. For certain aspects, such as the d-orbital occupation, one can directly use the model parameters; for others the electron-density-distribution maps have to be examined.

5.1. Atomic net charges

The number of valence electrons attributed to each atom may be defined in different ways.

From a multipole model refinement of the x-ray diffraction data this may be done by eliminating all the non-spherically symmetric terms from the multipole model (a so-called κ-refinement [22]): all parameters are kept fixed (scale factor, structural and secondary extinction parameters) with the exception of the Ni 3d ($P_{\mathrm{Ni}\,00}$) and Si total valence electron counts ($P_{\mathrm{Si}\,V}$) and the radial extension parameters, κ, for these two atoms. With this approach the total electron density is in reality projected onto normalized, spherically symmetric, atomic-like functions, and the coefficients represent numbers of electrons allocated to the individual atoms.

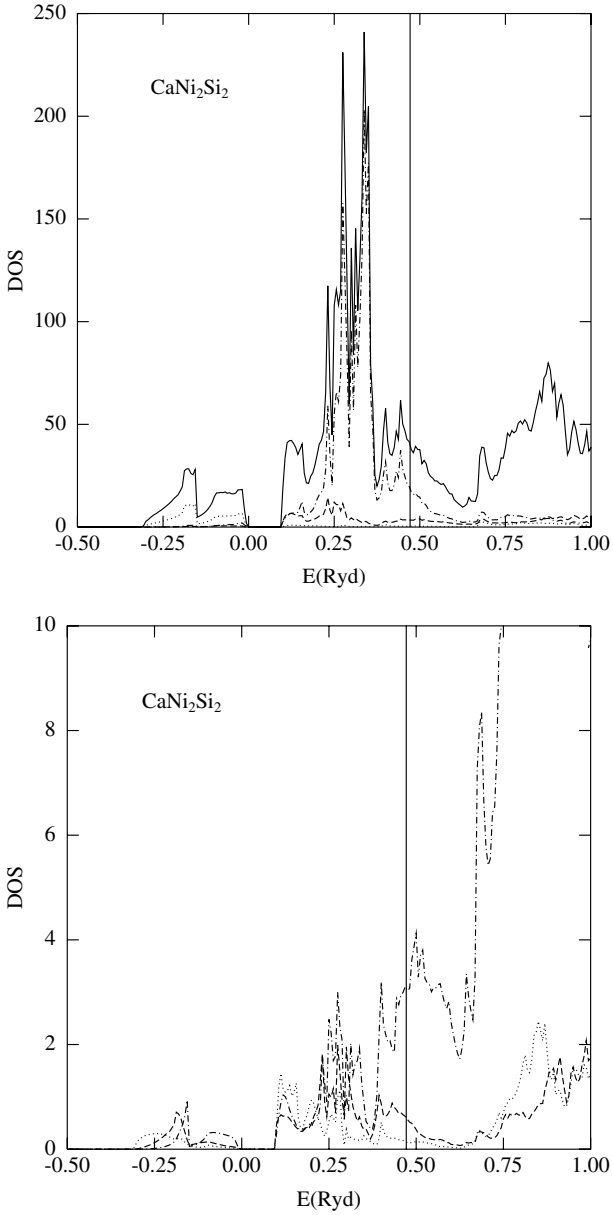

Figure 3. Top: the total DOS (full line) and local partial DOS components for Si s (dotted line), Si p (dashed line) and Ni d (dashed–dotted line). Bottom: the local partial DOS components for Ca s (dotted line), p (dashed line) and d (dashed–dotted line). Units: one-electron states per Rydberg and per unit cell.

Another approach is to integrate the total distribution of valence density according to the multipole model within spheres centred at the atoms. This has the advantage of an easy comparison with the results of LAPW-type calculations.

The resulting electron counts obtained from these approaches are reported in table 3. We first notice that the multipole model fitted to the experimental data yields 25.3 instead

of 30 valence electrons per formula unit. This lack of electrons is explained by the fact that the diffracted intensities are not very sensitive to diffuse components of the electron-density distribution. The κ-model projects out 28.6 electrons (see table 3).

Table 3. Atomic valence electron charges (net electron counts).

		Kappa model		Integration		
		Population	κ	R_{MT}	Q (x-ray)	Q (LAPW)
Ni	4s	1.0 (—)	1.0			0.55[a]
				1.06	9.0	8.45[b]
	3d	7.3 (1)	1.04 (1)			7.94
Si		6.0 (1.0)	0.91 (3)	1.06	2.3	1.78
Ca		0 (—)	—	1.59	<0	1.17

[a] Formally s- and p-type orbitals.
[b] Formally s-, p-, d- and f-type orbitals.

In the multipole model, the number of 4s electrons on Ni was, rather arbitrarily, kept equal to one; as their distribution is very diffuse, they only contribute little to the diffraction.

The discrepancy between these ways of counting the electrons is even more pronounced when comparing the results for Si; only about half of the electrons that the κ-model allocates to this atom are within the 'muffin-tin' sphere. The fact that these electrons have such a diffuse distribution leads also to quite inaccurate charges in the refinement with a standard error of 1.0 e^-.

For an isolated silicon atom in the ground state, the number of valence electrons within a sphere of radius 1.06 Å is 1.5. Therefore both the theory and the experiment indicate an electron transfer towards silicon that is more pronounced in the latter case.

For the nickel atom the FLAPW calculation predicts about as many electrons in the 3d shell as for the isolated atom. The experimental data correspond to a larger number of electrons within the muffin-tin sphere, but this is mainly due to a diffuse density which should not be characterized as 3d-like. The κ-refinement leads to a much smaller density, equivalent to 7.3 electrons. This is almost the same number as the one resulting from the complete multipole model refinement.

5.2. Individual d-orbital populations of the Ni atom

The valence electron-density distribution in the vicinity of the Ni ion may be considered to be mainly composed of contributions from the 3d orbitals and their hybridization with other more diffuse states. Because of the way in which we have modelled the electron density, mainly 3d–3d products will project out. It has been shown by Holladay *et al* [23] that in this case (assuming that the orbital moment is quenched) there is a one-to-one correspondence between the multipole expansion coefficient P_{lm} and the d-orbital population matrix. Because of the site symmetry there are no mixed-product terms when referring to a coordinate system having its axes parallel to the crystallographic axes. The resulting values are given in table 4. The populations corresponding to the (more standard) choice of axes with x and y pointing towards next-neighbour Ni ions are simply obtained by permuting the values for the $d_{x^2-y^2}$ and d_{xy} orbitals.

The anisotropy in the d-orbital occupation also appears clearly in the electron-deformation-density map (the total density minus superimposed independent-atom densities) shown in figure 2.

Table 4. d-orbital populations on Ni (standard errors are given in brackets).

d_{z^2}	1.57(3)
d_{xz}	1.76(2)
d_{yz}	1.76(2)
$d_{x^2-y^2}$	0.96(3)
d_{xy}	1.19(3)

It is observed that there are more electrons in the orbitals pointing out of the Ni layer. For the in-layer $d_{x^2-y^2}$ and d_{xy} orbitals there is a slight preference for pointing in the direction of the nearest Ni ions, though this difference is hardly statistically significant (it is controlled by one parameter in the model, P_{44+}, whose value differs from zero by a standard deviation of 1.3).

5.3. Valence electron density

Theoretical and experimental valence electron-density maps in the planes of interest, namely (100) containing Ca, Si and Ni, (110) containing Ca and Si and (001) through the Ni atoms, are shown in figures 4–6. The experimental maps are so-called *static maps*, i.e. they are corrected for thermal motions using a convolution approximation on an atomic level.

The experimental maps show pockets of non-physical negative density amounting to -0.05 electrons Å^{-3}. In general the experimental maps differ from the theory by less than

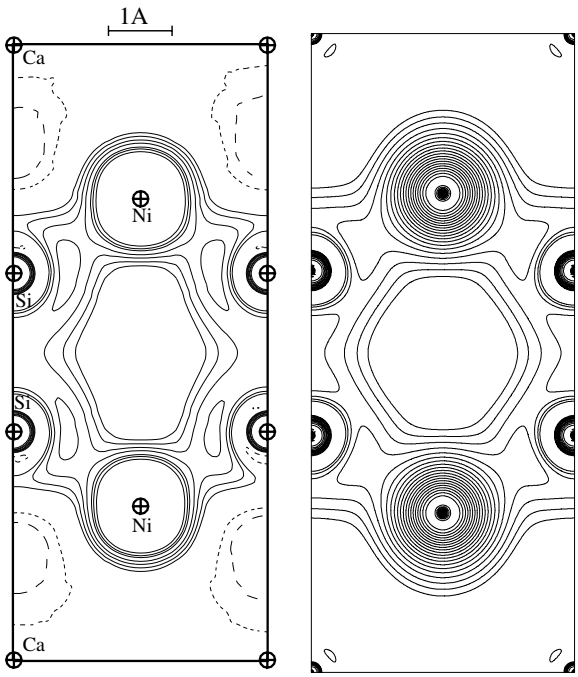

Figure 4. Experimental (left) and calculated (right) valence electron distributions in the (100) plane. A logarithmic grid of contour lines has been used ($x_i = 0.2 \times 2^{i/3}$ electrons Å^{-3}). The long broken line is at a density of -0.05 electrons Å^{-3}, the short broken line at 0 electrons Å^{-3} (see the text).

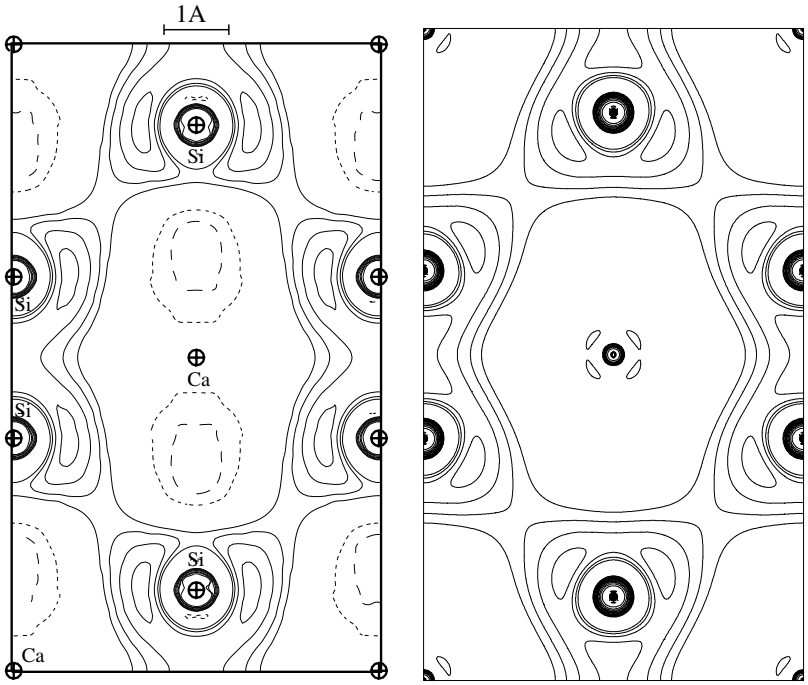

Figure 5. Experimental (left) and calculated (right) valence electron distributions in the (110) plane through the Si and Ca atoms. The same grid lines as in figure 4 have been used.

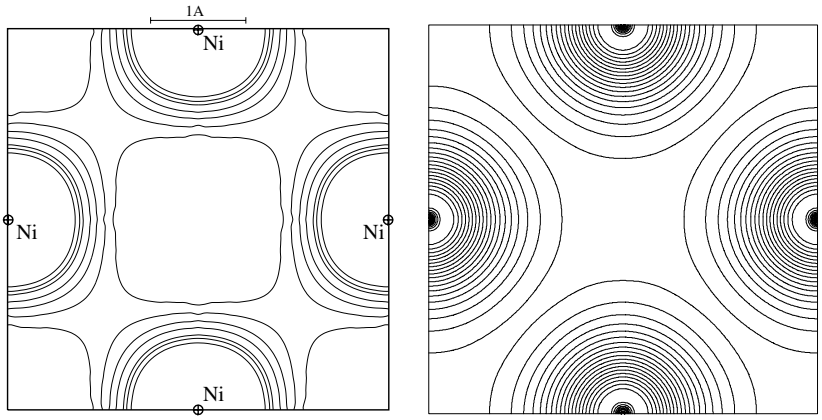

Figure 6. Experimental (left) and calculated (right) valence electron distributions in the (001) plane through the Ni atoms. The same grid lines as in figure 4 have been used.

0.1 electrons $Å^{-3}$. We estimate that the uncertainties in our static maps are of the order of 0.1 electrons $Å^{-3}$ correlated over the resolution length of the diffraction experiment of about 0.5 Å. This may partly explain the differences between the numbers of valence electrons inside the muffin-tin spheres and the lack of electrons in the unit cell. The latter point may also be due to a poor accuracy in regions of very flat distributions of electron density which only affect the scattering close to the forward direction, and that only weakly. We recall that the best agreement with the data is obtained with an empty valence shell for the calcium pseudo-atom.

While an accuracy of 0.1 electrons $Å^{-3}$ may account for the discrepancy between experiment and theory, one notices, however, qualitative differences, mainly in the Si–Si bond region ((100) and (110) sections) and in the (100) plane concerning the Si–Ni interaction. This may be due to a lack of accuracy for the weak reflections ($l = 8n \pm 1$) which are very decisive for determining the non-centrosymmetric component of the Si pseudo-atom density. If these reflections are included in the refinement, additional non-physical negative-density pockets appear near the nucleus of silicon, and this clearly shows that a reliable description of the electron density is only feasible if these reflections are measured with a very high accuracy. The negative pockets may also appear because of limitations in the multipole model; a model accounting for both the Si–Si nearest neighbours and the Si–Ni interactions requires two multipoles breaking the cylindrical symmetry about the Si–Si close contact. Owing to the high symmetry of the silicon site (point group $4/mmm$) the multipoles of lowest order with this property are y_{44+} and $y_{54+} \propto y_{44+}\, y_{10}$. The software is nevertheless limited to orders $l \leqslant 4$.

In fact multipoles of order higher than 2 project out d and f orbitals that are only weakly populated. As seen from figures 4–6, the bond critical point† between next-neighbour silicons is located outside the muffin-tin spheres, in a region in which the wavefunctions of the theoretical calculation are projected onto plane-wave basis functions. The corresponding electron density may be projected onto multipoles, but it is difficult to guess *a priori* the appropriate shape of the radial functions, in contrast to the in-sphere part which is mainly due to atomic-like s and p orbitals and expected to have a shape rather similar to those of the isolated atom. With these limitations in mind, the experimental electron-density maps are in good agreement with the theory. The theoretical electron density gives a more pronounced impression of a covalent character of the short Si–Si contact. This is in agreement with the observation that this distance varies little among the silicon-containing compounds of this structure type.

The only feature in the deformation-density map (figure 2) which deserves notice is the signature of the 3d-electron distribution of the nickel atoms.

In the nickel plane the density shows a deviation from circular symmetry with an extension in the direction of next neighbours in agreement what we observe in terms of the orbital populations, but opposite to what is found in the LAPW calculation.

In conclusion, we would like to stress the rather good agreement between experiment and theory. There is a tendency for the experiment to predict a somewhat stronger anisotropy of the nickel ion with close to single occupation of the d orbitals in the nickel plane. The experiment also seems to favour a slightly higher degree of delocalization of the electrons.

In order to be more conclusive about these trends, other compounds of this structural family must be studied, and it would be preferable if this was done with an improved experimental accuracy—something which, according to this study, should clearly be possible.

Acknowledgments

We thank HASYLAB/DESY for permitting us to use the synchrotron radiation facility. This work was partly supported by the Austrian Fonds zur Förderung der wissenschaftlichen Forschung (Project No P11393). Support from the Université Henri Poincaré, Nancy I, and the CNRS is acknowledged.

† A critical point is defined by having a gradient of the total electron density equal to zero. For a general discussion see [24].

References

[1] Ban Z and Sikirica M 1965 *Acta Crystallogr.* **18** 594–9
[2] Villars P and Calvert L D 1991 *Pearson's Handbook of Crystallographic Data for Intermetallic Phases* 2nd edn (Materials Park, OH: ASM International)
[3] Nagarajan R, Sampathkumaran E V, Gupta L C, Vijayaraghavan R, Prabhawalkar Bhaktdarshan V and Padalia B D 1981 *Phys. Lett.* A **84** 275–7
[4] Steglich F, Aarts J, Bredl C D, Lieke W, Meschede D and Franz W 1979 *Phys. Rev. Lett.* **43** 1892–6
[5] Szytuła A and Leciejewicz J 1989 *Handbook on the Physics and Chemistry of Rare Earths* vol 12, ed K A Gschneidner Jr and L Eyring (Amsterdam: Elsevier) pp 133–211
[6] Blaise A, Fåk B, Sanchez J P, Amoretti G, Santini P, Caciuffo R, Schmitt D, Malaman B and Venturini G 1995 *J. Phys.: Condens. Matter* **7** 8317–30
[7] Welter R, Venturini G, Fruchard D and Malaman B 1993 *J. Alloys Compounds* **191** 263–70
[8] Venturini G, Welter R, Ressouche E and Malaman B 1995 *J. Magn. Magn. Mater.* **150** 197–212
[9] Venturini G, Malaman B and Ressouche E 1996 *J. Alloys Compounds* **241** 135–47
[10] Hoffmann R and Zheng C 1985 *J. Phys. Chem.* **89** 4175–81
Zheng C and Hoffmann R 1988 *J. Solid State Chem.* **72** 58–71
Zheng C 1993 *J. Am. Chem. Soc.* **115** 1047–51
[11] Ishida S, Asano S and Ishida J 1986 *J. Phys. Soc. Japan* **55** 936–45
[12] Gustenau E, Herzig P and Neckel A 1997 *J. Solid State Chem.* **129** 147–56
[13] Gustenau E, Herzig P and Neckel A 1997 *J. Alloys Compounds* **262–263** 516–20
[14] Wimmer E, Krakauer H, Weinert M and Freeman A J 1981 *Phys. Rev.* B **24** 864–75
Jansen H J F and Freeman A J 1984 *Phys. Rev.* B **30** 561–9
[15] Hedin L and Lundqvist B I 1971 *J. Phys. C: Solid State Phys.* **4** 2064–83
Hedin L and Lundqvist S 1972 *J. Physique Coll.* **33** C3 73–81
[16] Blessing R H 1989 *J. Appl. Crystallogr.* **22** 396–7
[17] Hansen N K and Coppens P 1978 *Acta Crystallogr.* A **34** 909–21
[18] Clementi E and Roetti C 1974 *At. Data Nucl. Data Tables* **14** 177–478
[19] Dawson B 1967 *Proc. R. Soc.* A **298** 255–63
[20] Becker P J and Coppens P 1974 *Acta Crystallogr.* A **30** 129–47
[21] Jepsen O and Andersen O K 1971 *Solid State Commun.* **9** 1763–7
Lehmann G and Taut M 1972 *Phys. Status Solidi* b **54** 469–77
[22] Coppens P, Guru Row T N, Leung P, Stevens E D, Becker P J and Yang Y W 1979 *Acta Crystallogr.* A **35** 63–72
[23] Holladay A, Leung P and Coppens P 1983 *Acta Crystallogr.* A **39** 377–87
[24] Bader R F W 1994 *Atoms in Molecules: a Quantum Theory* (Oxford: Clarendon)